Chapter-4

Molecular interaction between bi-antennary phenylboronic acid and sialic acid

Chapter 4. Molecular interaction between bi-antennary phenylboronic acid and sialic acid.

4.1 Introduction

4.2 Materials and Methods

4.2.1 Molecular dynamics (MD) simulation

4.2.2 optimization

4.3 Results and discussion

4.3.1 Frontier Molecular Orbital analysis

4.3.2 Spectral analysis via vibrational assignments

4.3.3 Binding Energy

4.4 Conclusions

References

4.1 Introduction

Alteration of the glycosylation patterns which produces the co-translational and post-translational modification in neoexpression, underexpression or overexpression are hallmark of cancer [1]. These diverse processes are either found in the core or on the terminal structure of carbohydrates corresponding to the glycoproteins. Produced co-translation and post-translation structures often arise from the changes in expression levels of glycosylating enzymes in cancerous versus healthy cells [1, 2, 3]. Given the functional link between aberrant glycosylation and malignancy, therapeutics which blocks the formation of cancer-associated glycans possibly effects on tumour the progressions. The immune system can be recruited to the targeted cancer cells on the basis of their altered glycosylation. Glycosylation generally occurs through differential expression of glycosyltransferases, glycosidases and monosaccharide transporters within the cancer microenvironment. Often, it is implied that hypersialylation at the end of the chain and increased addition of the non-human sialic acid (N-glycolyl-neuraminic acid (Neu5Gc)) into cell surface glycans develop the cancer [4]. Sialic acid (SA) refers to a family of more than 50 configurations of the structures typically varying at the C5 position. [5,6]

There is a great diversity of cell-surface glycans each of which have characteristic structures with varying types of terminal or internal monosaccharide sequences [7]. SAs with a shared nine carbon backbone are a kind of anionic monosaccharide which usually occurs at the terminal end of several classes of cell surfaces. Secreted glycan molecules have gained special attention due to their crucial and distinctive roles in some biological and pathological events. [8] N-Acetylneuraminic acid (Neu5Ac) and N-glycolylneuraminic acid (Neu5Gc) are two major forms of SAs in most mammals, whereas the former one is almost the only form found in human body is Neu5Ac (Figure 1) [9]. For our whole study we continue the Neu5Ac

structure of SA, which is known as the alpha anomer. In the human body, the abnormal expression and distribution of SA on cell surfaces or in body fluids have been demonstrated to be closely associated with various diseases, including cancer, diabetes, cardiovascular and neurological diseases [10-13]. Moreover, SA has been identified as a tumor-associated antigen as its overexpression on the cell surface reveals the malignant and metastatic phenotypes for various types of cancers [13-15]. Therefore, the detection and monitoring of SA in biological samples or on living cell surfaces have great significance in terms of fundamental glycobiology research, clinical diagnostics as well as therapeutics. Figure 4.1 is a schematic representation to understand the structurally diverse SA family and glycans on cell surface.

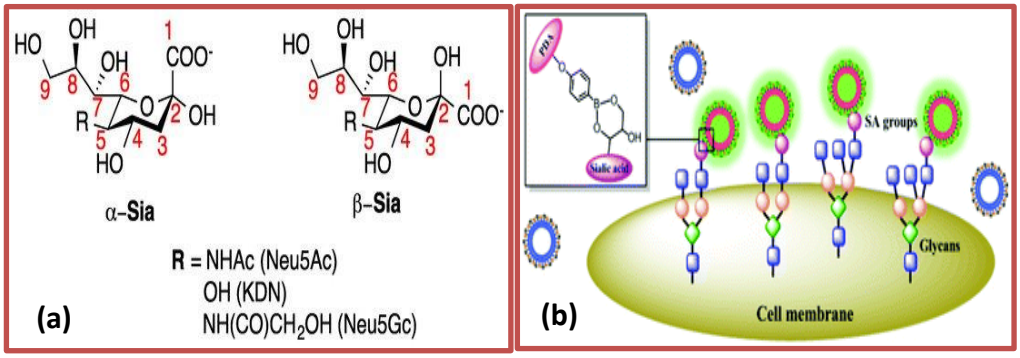

Figure 4.1: (a) Examples of the structurally diverse SA family. Where, alpha-anomer is the form that is found when sialic acid is bound to glycans and beta- anomeric configuration is in solvent [5], (b) Specific imaging of glycans on cell surface [6].

Chemical modification of monosaccharide structures are known to augment the immunogenicity of glycan based vaccines [16, 17]. Cancer associated hyper-sialylation affects the interaction of tumor cells with sialic acid binding lectins [18], particularly those responsible for maintaining the appropriate inflammatory environment [19]. In this context, perception of exploiting biological identification elements including those based on enzymes or sugar binding proteins (lectins) [20, 21] have been developed and are widely utilized. Synthetic chemosensors, however, are more desired in terms of the stability, low cost, and oxygen independence. As the SA expression on cell surface persists, particularly from the

perspective of early detection of malignant cell [22, 23, 24]; at the same time, SA-specific molecular recognition can also be exploited to selectively localize the therapeutic agents in the region of highly sialylated epitopes, thereby sparing the healthy cells [25]. SA can therefore be studied and explored with the help of the saccharides and mimetics [26, 27, 28] by experimental and theoretical approaches [21]. Saccharides and mimetics such as Galactose (Gal), Mannos (Man) and phenyleboronic acid (PBA) are most preferable ligands due to their dual approach of cationization and attachment to recognition of peptide while targeting the colon cancer cells. Phenylboronic acid (PBA) is known to form esters with SA between pH 2 and 12 [29, 30, 31]. At lower pH (2–8), the α-hydroxycarboxylate moiety at C_1/C_2 participates in the binding energy, whereas at pH >8 the interaction of PBA takes place at the glycerol site on the chain to give a five-membered ester at C_8 and C_9. Molecular docking studies also supported these results [29]. At physiological pH, carboxyl group acts as a negative charge center on the SA molecule and does not participate in the interaction [29].

SA-PBA complexation is favored by the trigonal form of binding, for which participation of multiple metastable binding sites along with intra-molecular stabilization via B-N or B-O interactions are crucial. However, experimental evidence suggests higher affinity interactions of the polyvalent saccharides with SA in cancer cells [22]. Our earlier studies show an enhancement in the SA-PBA interaction with a shift from mono- to bi-valent type of interactions [28]. Also, the binding constant shows the magnitude which is higher than that of monovalent interactions. Based on quantum mechanical calculations, we conclude that, saccharides (mannose and galactose) have high binding affinity for extra-cellular SA, specifically at tumor-relevant pH and temperature conditions [28]. Such binding can be further improved by increasing the valency of saccharide ligands [22]. With these insights, we have demonstrated the ability of bi-antennary ligands to achieve a high affinity interaction with the extra-cellular SA on a molecular level in this chapter. We employed the top scored

binding saccharide as input of subsequent MD simulations to provide a biological relevance and trajectory. We have presented the vibrational spectra, supported by potential energy distribution (PED) analysis. PED analysis of the theoretically calculated IR spectra forms the basis for the elucidation of future matrix isolation. In the last few decades, this type of interaction has been studied extensively utilized to perform DFT and MD simulations. Recently, a significant difference in the wild-type and ΔK9 form of thrombin was observed using combined molecular dynamics simulation and machine learning [32]. Jana et. al. performed a study to search highly specific, less toxic, non- (zinc-binding groups) ZBG inhibitors of matrix metallopeptidase 9 (MMP-9), on the basis of e-pharmacophore and ligand-based approaches to develop drug for the various disorders [33].

4.2 Materials and Methods

Every monovalent ligand and receptor complex was manually selected from the ChemSpider which is the free chemical structure database [34] and the bi-valent molecular structures were developed with the help of GAUSSIAN 09 suite gaussview. The entire complex, that is, the SA structure with bi-antennary ligands such as Gal, Man, and PBA was optimized in 6-31G basis set using GAUSSIAN 09 suite separately [35]. Becke's three parameter hybrid functional using the Lee-Yang-Parr correlation function (B3LYP) [25] was used to obtain the minimum global energy structure representing the ground state of the system . After the analysis of optimized complexes and on imposing the basis set superposition error (BSSE) [37] of intermolecular potential to the complex of SA with bi-antennary saccharides we continue with 2- Phenylboronic acid (2PBA) on the basis of the interaction energy. Quantum chemical properties such as atomic charge, electrophilicity [ω], chemical hardness[η], chemical softness[σ] and electro chemical potential [μ] [38] were calculated using equations presented in previous chapter. The frontier molecular orbital (FMO) analysis and Mulliken population analysis were performed for the elementary interpretation of static structure to describe the probability of electrostatic interactions respectively [39]. Vibrational

assignments and structural characteristics of the complex were performed to investigate the momentum [40, 41]. Electrostatic potential was estimated to calculate the charge distributions over the complex, PED (using VEDA 4 program) and energy of the determined structure were calculated using the first principles based Density Functional Theory (DFT) [42].

The IR and Raman spectra were generated with full-width at half maximum (FWHM) of 10 cm^{-1} as pure Lorentzian bands from the calculations. Also, the simulated Raman spectra was obtained by computing the Raman activities (R) converted to relative Raman intensities (IR) as represented in equation below; [43, 44]

$$IR = [f(V_0V_i)^4R]/[V_i\{1 - exp(-hcV_i/kT)\}] \quad (4.1)$$

Where, V_0 is the exciting frequency in cm^{-1}, νi is the vibrational wavenumber of the i^{th} normal mode, h, c and k are universal constants, and f is the suitable scaling factor suitably chosen for all the peak intensities.

The optimized ground state structures were placed together approximately at a distance of 2 to 3 Å in absence of any external force, that is, under ideal unconstrained conditions as receptor and ligand. This creates a state such that, the ligands and receptor's most active sites are situated closer to each other. Difference between energy of complex and sum of energies of its total fragments are calculated in the form of interaction energy E_{int}^{AB} of ligand target binding.

$$E_{int}^{AB} = E_{AB}^{opt} - (E_A^{opt} + E_B^{opt}) + E_{AB}^{BSSE} \quad (4.2)$$

Where, E_{AB}^{opt}, E_A^{opt}, E_B^{opt} and E_{AB}^{BSSE} are complex energy, ligand energy, receptor energy and basis set superposition error respectively. Theoretical ab-initio and DFT studies were carried out on 2PBA to obtain reliable, accurate vibrational assignments and structural characteristics of the compound. Newtonian mechanical properties are examined by the newton's second law of motion based molecular dynamic simulation to evaluate the dynamical movement at microscopic level.

4.2.1 Molecular Dynamics (MD) Simulations

As discussed previously, drug-discovery is a time-consuming process, and to overcome this; various computational methods have been employed like Structure based drug discovery (SBDD) and ligand-based drug discovery (LBDD) which rely on the structure of the target and ligands respectively. Although, there are several methods available, molecular dynamics (MD) simulations have turned out to be essential technique in the field of designing new bioactive compounds. MD simulations explain the crucial role of protein conformational flexibility in binding to the ligand or vice-versa as treating flexibility has always been an issue. Also, the MD simulations have been successfully employed to observe the molecular interactions.

MD simulations were performed for the SA- 2PBA complex. Once the initial minimization process was completed using steepest descent and conjugate gradient method the system was pulled into the type of TIP3P water molecules [45] with orthorhombic periodic boundary condition to describe how the system behaves on its boundaries (for all times) and initial conditions, that specify the state of the system for an initial time t=0. After the optimization, complex was subjected to NVT ensembles as Berendsen barostat [46] and NPT ensemble as Nose-Hoover thermostat [47] for 300K over 1.2ns and 5ns, 15ns and 25ns simulation time respectively. Total 500 frames have been taken out along the coordinates for all NPT simulation time periods. Trajectory time for 5ns, 15ns and 25ns simulations were 10ps, 30ps and 50ps with 1 bar pressure and 300K temperature. To measure the similarity in three-dimensional structure root mean square deviation (RMSD) was calculated for terminal frames of three simulations. OPLS_2005 force field mathematical model was used to approximate

the atomic-level forces acting on the simulated molecular system [48]. The RMSD last retrieved frame at time t500 with respect to a given reference structure (first frame) at time t1:

$$\text{RMSD (t1,t2)} = \sum_{Ni=1}^{N}(Xi(t2) - Xi(t1))1/2 \quad (4.3)$$

Xi (t) is position of atom i at time t and N is the total number of atom in the complex The first frame of trajectory (t1) is used as a reference to calculate the values of RMSD.

4.2.2 Optimization

The present work utilized a focussed dataset made up of the experimental activities of the 3 selected enzymes. The validation of these structures is generally performed to evaluate the quality of the model. However, an essential attribute of a reliable model is to predict the internal and external dataset appropriately. In this chapter, to perform the validation process we optimized all the structures using Gaussian under the first principle based density functional theory on the basis of above defined parameters in methodology section. On successful optimization each ligand was organized with receptor manually with distance of 2 to 2.2 Å. Suitable interacting complex or lead complex was selected to perform further simulations procedure. QM calculation was applied to find the significance sensitivity against the enzyme, whereas the MD simulations were performed to calculate the force on the *SA* with respect to the time. After the MD simulation process, we chose the last frames of all time slots to compare the binding affinity with the help of the DFT with same parameters. Optimized structure at 15 ns was found the best candidate which shows the good binding affinity as compared to others.

4.3 Results and discussion

MD simulations and QM (DFT)/MM calculations have been together applied to understand the interaction of bi-antennary saccharides such as Gal, Man and PBA with SA interactions. The inter-atomic potential of complexes depends on channel of the 3D molecular formation (Figure 4.2). The content of high SA concentration cell suggests that there are auxiliary

functions to express the tumor cells when receptor binds competitively and comparably with higher affinity to bi-antennaries such as, GAL, MAN and PBA. Among all the bi-antennaries saccharides 2PBA mimic of saccharide is of primary interest to probe the impact of SA activators, and interacting affinity of this ligand to cellular SA domain. The three complexes were simulated and compared to each other. The selected bi-antennary PBA saccharide with SA was simulated for various time intervals and their behaviour was analysed in the presence of the water molecules using VMD-1.9.2 [49] and GAUSSIAN-09. Resulting data reveals that, the hydrogen bonds arise during the reaction.

Table 4.1. Presents the distance between two molecules corresponding to the optimized geometry of complexes of single antennary in comparison with the bi-antennary saccharides using DFT. Galactose with declared environment was chosen as the prime single antennary molecule for the best interacting ligand for SA target [28].

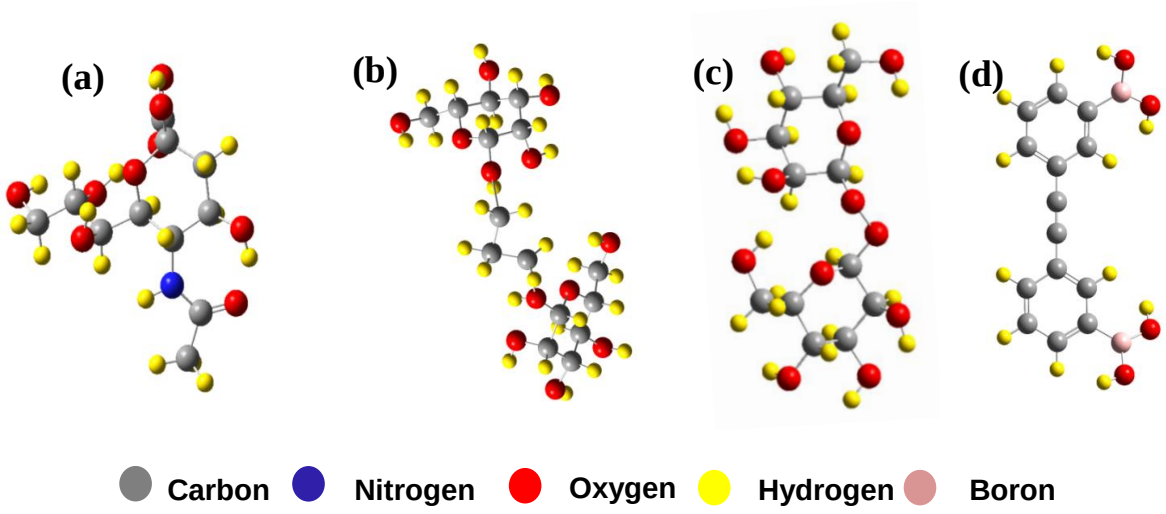

Figure 4.2: Molecular configuration of sialic acid (a) defined as a target structure, where biantennary Gal (b), biantennary Man (c) and biantennary PBA (d) play the role as ligands.

Table 4.1: Value of Binding energy, Highest occupied molecular orbital (HOMO), Lowest unoccupied molecular orbital (LUMO), band gap, Hardness, Softness, Chemical potential, Electrophilicity. Values mentioned in brackets represent the interaction of SA with monovalent saccharides [28].

Properties	**SA + Bi-antennary Galactose**	**SA + Bi-antennary Mannose**	**SA + Bi-antennary PBA**
$E_{binding}$(kcal/mol)	49.8781 (-31.7353)	-54.9871 (-23.8794)	-244.9476 (164.4198)
HOMO	-0.1926 (-0.1242)	-0.1529 (-0.1235)	-0.2254 (-0.1083)
LUMO	-0.0366 (-0.0953)	-0.0396 (-0.0667)	-0.0207 (0.0572)
HLG	0.1559 (0.0289)	0.1926 (0.0568)	0.2046 (0.0511)
Distance (Å)	2.74	2.47	1.80
Hardness (η)(eV)	0.078	0.0566	0.102
Softness (σ)(eV)	6.4102	8.8339	4.9019
Chemical Potential (μ)(eV)	0.1146	0.0962	0.12305
Electrophilicity (ω)(eV)	0.084186	0.0081	0.0742

Furthermore, the table 4.1 represents the comparable electronic properties of bi-antennary with SA complexes. Here, 2PBA stands out prominently due to the binding energy and distance between the molecules. Also, there's a significant difference in the binding energies of single antennary and bi-antennary PBA. But, it is remarkable to note that, in context of single antennary the bond length exhibits best binding configuration as compared to others in the range. On the other hand, the bi-antennary PBA binds with SA strongly which is also evident from the experimental study of David et. al. (2002) [22]. The resulting complex is attributed to the fact that, the bi-antennary galactose is highly flexible due to hydrophobic spacer arms that allow variation of their intergalactic distance and geometries which confirms the interaction between oligomeric structure and galactose.

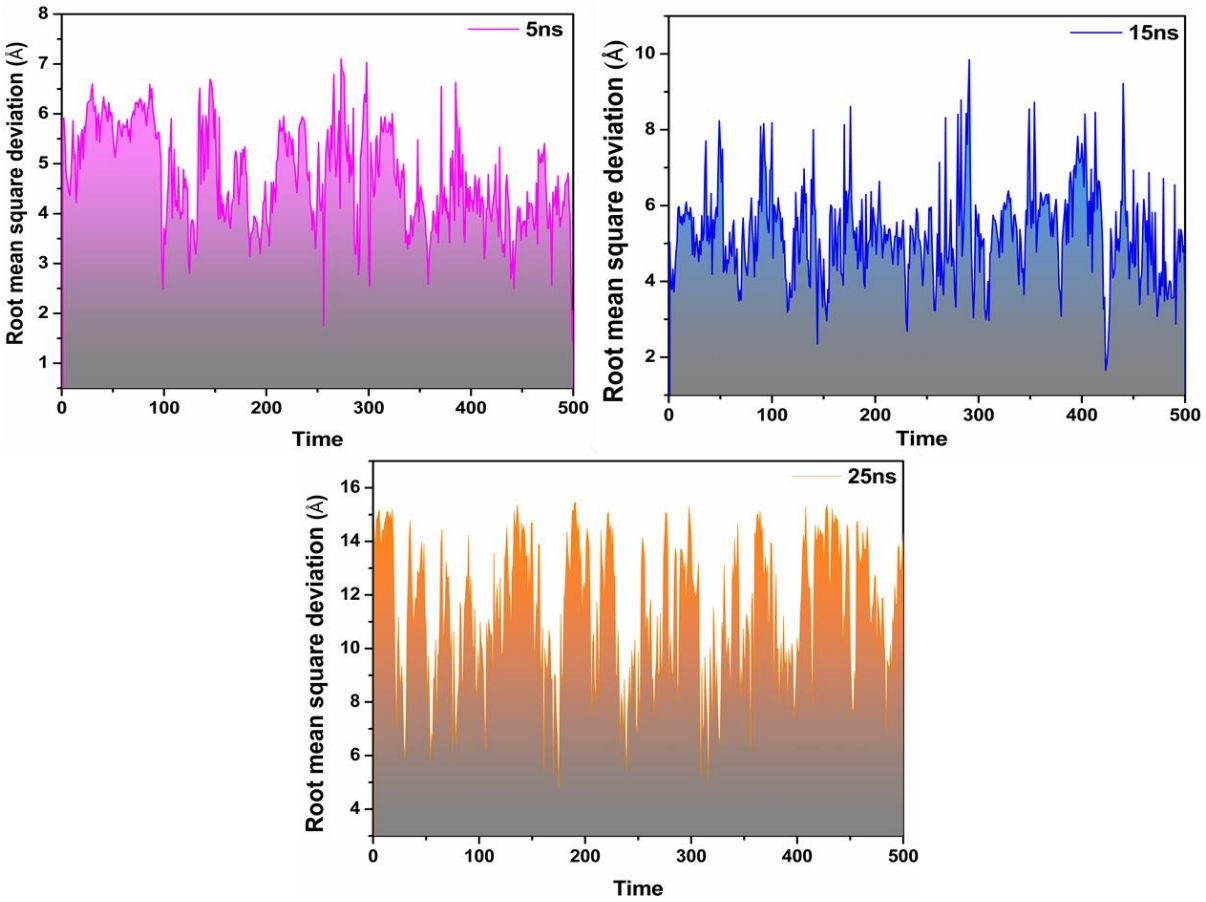

Figure 4.3: Time course of the root mean square deviation (RMSD) for MD simulations of 5 ns (pink) 15 ns (blue) and 25 ns (orange) of SA with Bi-antennary PBA. The RMSD of 25 ns is very high than 5 ns and 15 ns [28].

Figure 4.3 represents the RMSD plots which depict the performance of bi-antennary saccharides Gal, Man and PBA as good inhibitors. From all the contestant bi-antennaries, PBA turns out to be the best inhibitor against SA (as shown in Figure 4.2). The plots in Figure 4.3 show the accounted peaks of RMSD data which includes the 5, 15 and 25 ns duration of simulation. Comprehensive data of 500 trajectories separated by the X- axis and Y- axis represent corresponding time and deviation. With increase in the time-lag between configurations, variation in the RMSD values are evident. We find that, for multiple time periods, SA and 2PBA remained stable as shown using RMSD plots (Figure 3(a-c)). In principle, lower RMSD value exhibits higher stability and corresponding ground state energy. Moreover, the distance between constituents of the complex is 1.80 Å (Table 1). Although, there are minor variations at these time scales; the values range from 7.12 to 15.46 Å. Here

25 ns is not as stable as compared to the other time scales, hence we can say that, 15ns and 5ns configurations are the best for further analysis since, most of the dimers grow during the simulation times.

Table 4.2: Calculated the Binding energy expressed as a kcal/mol, as well as Hardness, Softness, Chemical potential and Electrophilicity of receptor SA against Bi-antennary PBA for 5ns, 15ns and 25ns complex.

Properties	**5ns**	**15ns**	**25ns**
$E_{binding}$(kcal/mol)	-176.4236	-181.2479	-175.4472
Distance (Å)	1.6278	1.579	1.6348
Hardness (η) (eV)	0.0260	0.0173	0.0285
Softness (σ) (eV)	19.2307	28.9017	17.5438
Chemical potential (μ) (eV)	0.08848	0.08871	0.09299
Electrophilicity (ω) (eV)	0.15055	0.22744	0.15170
RMSD (Å)	7.12	9.84	15.46

Electron deficient chemicals (also known as electrophiles) react with compounds that have one or more unshared valence electron pairs. The corresponding energies of the frontier molecular orbitals (ELUMO and EHOMO) are known which can be utilized to calculate the corresponding hardness (η) and softness (σ) of the complex. Within this context, softness is an index of relative ease with which, electron density is transferred from a nucleophile to electrophile during covalent bond formation. Hardness on the other hand is lower since several structures acquire more conductivity and vice versa with softness. As far as the hardness and softness are concerned, there is a clear disagreement with the ideal case (as shown in Table 4.1). The hardness of bi-antennary galactose, mannose and PBA is 0.078 eV, 0.0566 eV and 0.102 eV respectively while, the softness is 6.4102 eV, 8.8339 eV and 4.9019 eV respectively (Table 4.1). Theoretically, our study follows the conductivity surge at 15ns structure (with 0.0173 eV, Hardness and 28.9017 eV softness as shown in Table 4.2.) Moreover, the structure has highest electrophilicity, which shows the ability to donate electrons with 0.22744 eV value. These parameters are related to the rate of

adduct-forming reaction. Specifically, the electrophilic index (ω) is a comprehensive measure of electrophilicity that combines softness and chemical potential (μ). These data collectively show that, the hardness of best bound complex is reduced approximately by 33% at 5ns and 39% at 25 ns.

4.3.1 Frontier Molecular Orbital analysis

HOMO represents the ability to donate the electron density to form a bond while, LUMO represents the lowest lying orbital that is empty, so energetically it is convenient to add more electrons into this orbital. HOMO and LUMO are important to analyse the chemical reactivity thus, playing a decisive role in computing optical and electronic properties of molecules (as shown in Figure 4.4). Lower band gap indicates the possibility of higher charge transfer potential inside the receptor and it is related to higher interaction energy. For the mono-valent configurations, the band gap for PBA and Gal was found as 0.0511 and 0.0289 eV, respectively (as represented in Table 4.1).

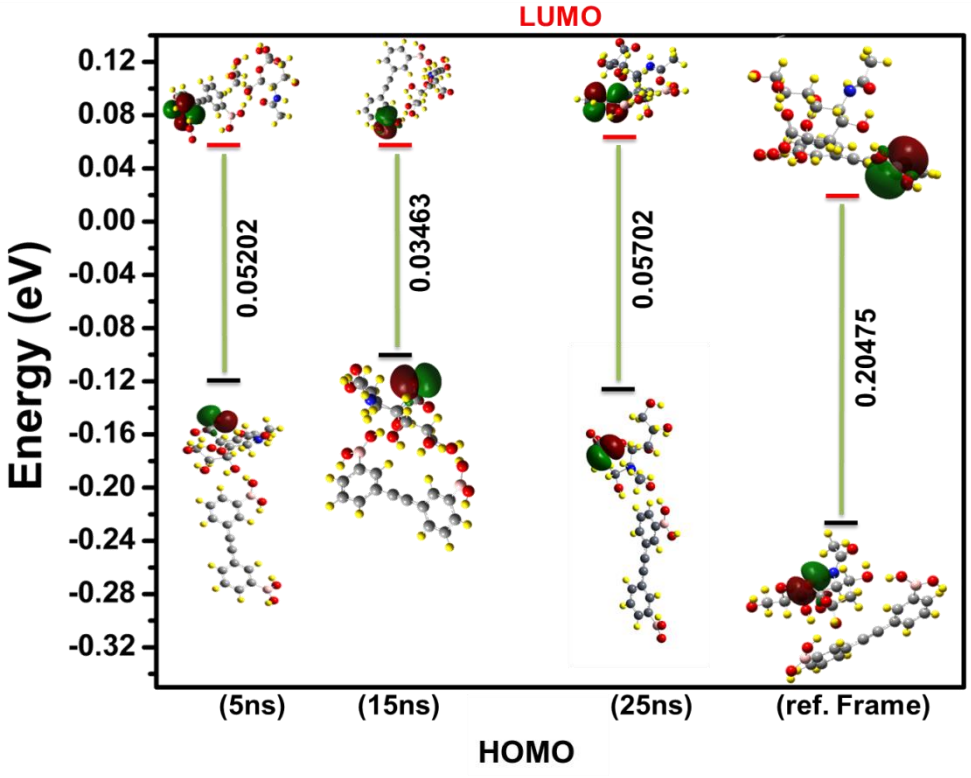

Figure 4.4: Atomic orbital HOMO and LUMO composition of frontier molecular orbital at, 5ns, 15ns and 25ns complex frames of SA against Bi-antennary PBA.

Figure 4.4 represents the energy gap of the complex, before and after simulation at different time periods. At 15 ns, the complex achieves highest stability and conductivity with least band gap of 0.035 eV resulting into a strong binding as compared to the other time dependent structures. This might be due to some external potential. At different time dependent complexes, the surface reactivity goes with the flow of binding energy (as shown in Table 2).

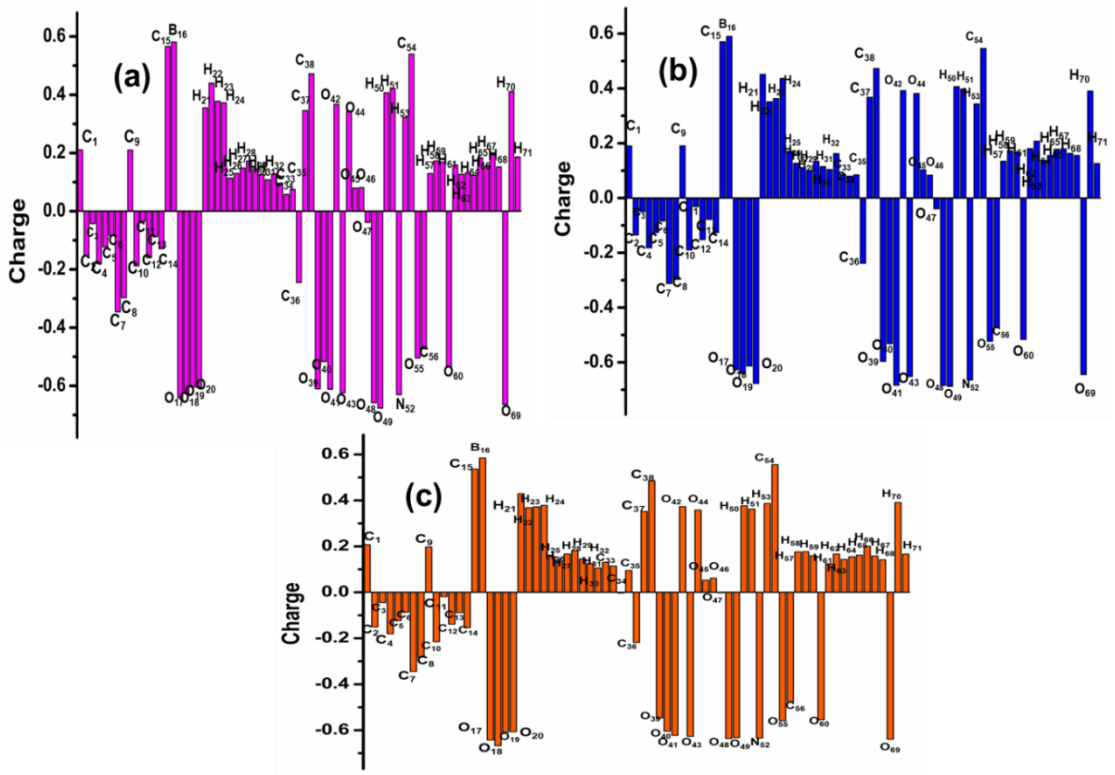

Figure 4.5: Evolution of the predictivity of the Mulliken charge during (a) 5ns (b) 15ns and (c) 25ns complex simulation time frames of SA-Bi-antennary PBA.

We consider the Mulliken population analysis (MPA) [50] which reproduces the chemical trends in well-understood small molecules where atomic populations can be reliably predicted using well-known quantitative and qualitative chemical concepts like atomic electronegativity and inductive effects. Although, Mulliken atomic charge is not investigable, but it can be used as comparable value to yield the consequential knowledge of molecular reactivity and various other properties which are dependent on it. At various glycosylation sites, single antennary contradicts bi-antennary glycans irrespective of the glycoprotein. In the 5ns system, maximum negative charge was found on O_{49} (-0.676785) and

O_{69} (0.664322) which may be attributed to the sharing of lone pair of electrons with neighbouring atom H_{22} (0.4401). The O_{49} site is a member of π electron system and is excessively electron deficient atom. Further, in the 15 ns simulation system, O_{49} (-0.6879) and O_{41} (-0.6839) carry negative charge which may also share electrons with H_{24} (0.4365) and H_{21} (0.4512). Whereas in the 25 ns system, most negative charge holder atoms are O_{40} (-0.6045) and O_{55} (-0.5585). Here, O_{40} is a π electron atom while the O_{55} may share the electrons with H_{21} (0.4287). The remaining hydrogen and nitrogen atoms carry positive and negative charges, respectively. Comparatively, there is a maximum change of absolute charge in all time scales. H_{24} to C_{35} and O_{47} show irregular behaviour throughout the simulation. C_{34} atom carries negative charge (-0.0035) in 25 ns structure whereas for 15 ns it carries positive charge (0.07969). This change in the negative to positive is consistent with the prediction of electrophilic and nucleophilic sites on the basis of molecular electrostatic potential surface.

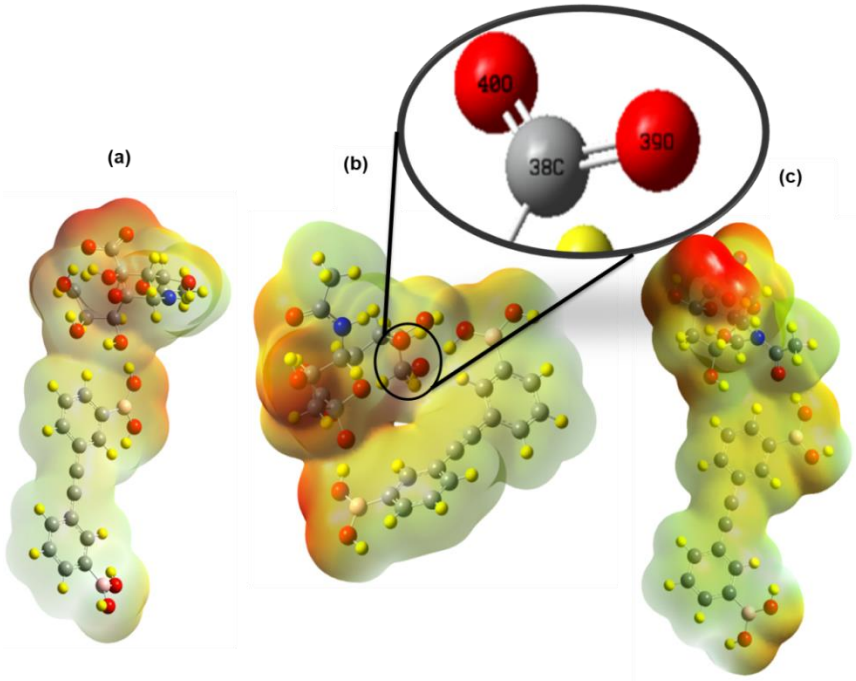

Figure 4.6: MEP of (a) 5ns (b) 15ns (c) 25ns complex of SA-Bi-antennary PBA.

Molecular electrostatic potential (MESP) [50-53] at a point in the space around a molecule gives an indication of the net electrostatic effect produced at that point by the total charge

distribution (electron + nuclei) of the molecule and correlates with dipole moments, electro negativity, partial charges and chemical reactivity of the molecule. It provides a visual method to understand the relative polarity of the molecule. An electron density isosurface mapped with electrostatic potential surface depicts the size, shape, charge density and site of chemical reactivity of the molecule. The calculated MESP is represented in figure 4.6, the coloured surface and 3D MEP show different values of electrostatic potential on the molecular surface. The blue colour indicates electron deficiency or partially positive, while the red colour represents electron rich or negative regions. Yellow and green colours show the slightly electron rich and neutral region respectively.

The colour coding of map ranges from -0.174 to +0.174 a.u., -0.175 to +0.175 a.u., and -0.165 a.u. to +0.165 a.u. at 5ns, 15ns and 25ns respectively for the corresponding complex. It is evident from Figure 4.6(a), (b) and (c) respectively that, the negative region is concentrated over C_{38}, O_{39} , O_{40}, O_{41} and O_{43}. This indicates that, the region around C_{38}, O_{39}, O_{40} and O_{41} is most suitable for electrophilic attack while, the region around H_{57}, H_{58} and H_{59} is slightly light blue which indicates that it is most suitable site for nucleophilic attack. The rest of the molecule is light green which indicates the electrostatic potential between the two extremes. The non-red and non-blue regions corresponding to mediatory potential; forms the crucial part of MEP which implies that, the electronegativity difference in the molecule is not very great.

4.3.2 Spectral analysis via vibrational assignments

Table 4.3: Assignment of the vibrational frequencies at 5ns, 15ns and 25ns complex of SA Bi-antennary PBA [56].

Configuration	Frequency cm^{-1}	Observed bands Intensity (A.U.)	Vibrational Bond	Assignments	PED(%)
5ns	3300	152.71^{IR}	O(48)-H(50) N(52)-H(53)	Antisymmetric	97 10
	3129	2121.71^{IR}	O(69)-H(70)	Rocking	93
	3124	117^{IR}	H(64)-C(36)-H(68)	Antisymmetric	88
	3071	116.76^{R}	C(46)-H63	Antisymmetric	50
	3059	136.60^{R}	H(59)-H(57)-C(56)-H(58)	Symmetric	38
	3045.64	111.93^{R}	C(39)-H(66)	Antisymmetric	95
	2980.48	1382^{IR}	O(49)-H(51)	Scissoring	93
	1491.25	131.96^{IR}	H(41)-C(45)	Rocking	39
	1464.25	313.72^{IR}	H(71)-C(45)-O(69)	Rocking	18
	1323.02	297.53^{R}	H(53)-N(52)-C(54)	Rocking	15
	1293.71	438^{IR}	C(46)-H(63) C(47)-H(62) C(45)-H(71) C(33)-C(45)	Rocking	18 12 12 18
	1177	188.33^{R}	C(34)-C(33)-C(45)	Rocking	23
	1173.37	657.62^{R}	C(45)-H(71)	Rocking	10
	1202	338.67^{R}	O(69)-H(70)	Rocking	17
	990.13	145.07^{IR}	C(45)-H(71)	Rocking	27
	935.02	296.01^{IR}	C(33)-C(45)-C(46)	Rocking	18
	923.46	279.21^{IR}	H(61)-C(47)-H(62)	Symmetrical	12
			C(33)-C(45)-C(46)	Antisymmetric	35
	798.70	125.61^{IR}	N(52)-H(53) C(34)-N(52)-C(54)	Rocking	20 13
	577.58	127.27^{IR}	C(46)-H(63) O(69)-H(70)	Rocking	27 21
	363.19	104.20^{IR}	O(43)-H(44)	Rocking	67

15ns	4066.44	108^{R}	O(43)-H(44)	Antisymmetric	89
	4020.48	199.88^{IR}	O(69)-H(70) O(48)-H(50)	Antisymmetric	74 72
	3984.28	150.20^{IR}	O(41)-H(42)	Antisymmetric	82
	3134	115.39^{R}	H(68)-C(36)-H(64) N(52)-H(53)	Symmetric	35 61
	3086	117.60^{R}	H(57)-C(56)-H(59)	Symmetric	10
	1830	290.51^{IR}	O(39)-C(38)-O(40)	Antisymmetric	17
	1766.36	193.32^{IR}	N(52)-C(54)-O(55)	Antisymmetric	18
			H(58)-C(56)-H(53)	Scissoring	41
	1599.52	158.12^{IR}	N(52)-H(53)	Rocking	12
	1427.76	115.80^{IR}	C(33)-H(65)	Rocking	16
	1121.30	107.06^{IR}	C(36)-H(64) O(41)-H(42)	Rocking	12 23
	1079.69	179^{IR}	O(49)-H(51) O(48)-C(40) C(46)-H(63)	Rocking	56 36 15
	-653.69	165.20^{IR}	O(43)-H(44)	Rocking	-
	-676	180.65^{IR}	O(43)-H(44)	Rocking	-
25ns	3874.18	151.20^{IR}	O(41)-H(42)	Antisymmetric	96
	3034	125.39^{R}	H(68)-C(36)-H(64) N(52)-H(53)	Symmetric	23 36
	3098.15	138.60^{R}	H(57)-C(56)-H(59)	Rocking	13
	1820	291.01^{IR}	O(39)-C(38)-O(40)	Antisymmetric	20
	1786.46	193.34^{IR}	N(52)-C(54)-O(55)	Antisymmetric	20
	1620.52	168.12^{IR}	N(52)-H(53)	Rocking	56
	1427.76	115.80^{IR}	C(46)-H(63)	Rocking	23
	1121.30	107.06^{IR}	C(36)-H(64) O(41)-H(42)	Rocking	20 56
	1189.69	189^{IR}	O(49)-H(51) O(41)-C(42)	Rocking	52 21
	567.58	128.37^{IR}	C(46)-H(63) O(69)-H(70)	Rocking	38 46

The computed geometrical parameters are good approximations and they form the basis to further calculate the parameters such as, Raman and IR vibrational frequencies as represented in Table 4.3. The vibrations in the systems are mostly governed by the C-C bonds and mostly exist in the region 1000 to 1300 cm^{-1} [56]. From the present analysis, the vibrations in receptor molecule are observed at 1297.71 cm^{-1} with rocking IR vibrations bands due to C_{33}-C_{45} atoms. Based on these data we assure that, the theoretical values support the experimental data [56]. The N-H stretches of amine group is generally found in 3000 to 3500 cm^{-1} region [56]. These vibrations have been arising due to the antisymmetry of N-H bond at 3300 cm^{-1} (due to N_{52}-H_{53}) region with 152.71 cm^{-1} IR intensity and 97% participation. The region 100-1300 cm^{-1} exhibits vibration modes due to the O-C bonds. This is evident at 5ns complex where, the band at 1173.37 cm^{-1} is due to O_{39}-C_{38} atoms with 657.62 cm^{-1} IR intensity and 10% involvement of rocking vibrations. Whereas, in the 15ns structure the vibrations are observed at 1079.69 cm^{-1} with 179 cm^{-1} IR intensity between O_{48}-C_{40} and O_{49}-H_{51} atoms with 36% and 56% PED respectively. The C-C rocking vibration mode is evident at 1293.71 cm^{-1} with 438 IR intensity due to C_{33}-C_{45} atoms and 18% PED. Based on the intra-molecular interaction, H_{21}-O_{41} and H_{24}-O_{49} atomic bonds form at 25ns. The C-C-C, H-C-H and C-N-C triad vibrations exist at 1177 cm^{-1}, 3124 $cm^{-1}$and 798.70 cm^{-1} respectively.

4.3.3 Binding Energy

The 2PBA-SA system provides an excellent test among all complexes. On the basis of dynamical studies of inhibitor-SA complexes, it has been suggested that, an inhibitor embedded in the receptor is transferred to the active site of the receptor surface. Table 4.1. shows the binding energy of SA with single-antennary, bi-antennary saccharides and mimetics [28]. Experimental studies also support the strong binding affinity of receptor with bi-antennary saccharides and mimetics [22]. The total ligand enzyme binding energy can be

calculated using equation 4.2 mentioned in the methodology section. It is to be noted that, the mimic as compared to 2PBA show the highest affinity for binding than the single antennary saccharides [28]. These calculations of the interaction energies are without considering biological environment, such as water and body temperature. Therefore to have near to real biological environment we have further simulated full complex in the presence of water molecule at different body temperature and pressure. Based on the evaluation of the data for bi-antennary case, further simulations have been performed on 2PBA and SA complexes which show instant binding in the absence of biological environment. We found that, the biological environment affects the binding which is consistent with our chapter 3. The binding energy reduces to -181.25 kcal/mol from -244.94 kcal/mol (≈26%) as evident from Table 4.2. This can be due to the fact that, it does depend on the type and number of bound sugar residue per molecule [22]. We reframe our discussion in this case to MD simulations only at 5ns since the simulations at different time scales yield no comparative variations in properties.

4.4 Conclusion

Density functional calculations based electronic properties, FMO, Mulliken charge, electro static potential, binding energy and vibrational spectra of bi-antennary and SA molecule is analysed. In this chapter we have investigated the electronic properties and binding energies of bi-antennary saccharides such as, galactose and mannose and the mimetic phenyleboronic acid with receptor molecule SA. As a result of this, we found that, 2PBA shows strong binding affinity with SA molecule. All calculations are carried out within the framework of dispersion corrected density functional theory and Newton's second law based molecular dynamics simulations. Further to prove the accuracy and the reliability, we continue the structure evaluation process at different time scales to get better conformity in order to explore SA in the presence of biological environment. Our results indicate that, in

the presence of strong interaction energy, bi-antennary PBA molecules would spontaneously move towards the SA at 15ns as compared to 5ns, 15ns and 25ns time scales. Binding energy was found to be -181.2479 kcal/mol with 1.579(Å) distance which shows that, the bi-antennary PBA quickly interacts with SA. The interaction between electron donor H_{24}, H_2 and electron acceptor π bonded O_{49} and O_{41} leads to the overall stability of the system. The MEP further suggests that, the negative potential is concentrated over lone pair of electrons in oxygen atom making them active sites for nucleophilic attack. The decreased HOMO–LUMO energy gap is the evidence of charge transfer interaction between donor and acceptor molecules. We finally conclude that the functional information on these interactions can contribute to the development of practically useful ligands which can be employed as therapeutic tools.

References

[1] D. H. Dube and C. R. Bertozzi, Nat. Rev. Drug Discov. **4**, 477 (2005).

[2] H.-B. Guo, A. Nairn, K. Harris, M. Randolph, G. Alvarez-Manilla, K. Moremen, and M. Pierce, FEBS Lett. **582**, 527 (2008).

[3] S. Hakomori, Proc. Natl. Acad. Sci. **99**, 10231 (2002).

[4] O. M. T. Pearce and H. Läubli, Glycobiology **26**, 111 (2016).

[5] A. Varki, R. D. Cummings, J. D. Esko, P. Stanley, G. W. Hart, M. Aebi, A. G. Darvill, T. Kinoshita, N. H. Packer, J. H. Prestegard, and others, *Essentials of Glycobiology*, 3rd edition. Cold Spring Harbor (NY): Cold Spring Harbor Laboratory Press (2015).

[6] S. S. Park, Vaccines **7**, 171 (2019).

[7] A. Varki, Nature **446**, 1023 (2007).

[8] N. M. Varki and A. Varki, Lab. Investig. **87**, 851 (2007).

[9] P. Tangvoranuntakul, P. Gagneux, S. Diaz, M. Bardor, N. Varki, A. Varki, and E. Muchmore, Proc. Natl. Acad. Sci. **100**, 12045 (2003).

[10] A. Cazet, S. Julien, M. Bobowski, J. Burchell, and P. Delannoy, Breast Cancer Res. **12**, 204 (2010).

[11] S. N. Chari and N. Nath, Am. J. Med. Sci. **288**, 18 (1984).

[12] K. P. Gopaul and M. A. Crook, Clin. Biochem. **39**, 667 (2006).

[13] A. Varki, Trends Mol. Med. **14**, 351 (2008).

[14] E. Köko\uglu, H. Sönmez, E. Uslu, and I. Uslu, Cancer Biochem. Biophys. **13**, 57 (1992).

[15] M. Li, L. Song, and X. Qin, J. Biosci. **35**, 665 (2010).

[16] P. O. Livingston, Immunol. Rev. **145**, 147 (1995).

[17] L. M. Krug, G. Ragupathi, K. K. Ng, C. Hood, H. J. Jennings, Z. Guo, M. G. Kris, V. Miller, B. Pizzo, L. Tyson, and others, Clin. Cancer Res. **10**, 916 (2004).

[18] Y. J. Kim and A. Varki, Glycoconj. J. **14**, 569 (1997).

[19] E. Rodrigues and M. S. Macauley, Cancers (Basel). **10**, 207 (2018).

[20] S. Wang, Y. Wen, Y. Wang, Y. Ma, and Z. Liu, Anal. Chem. **89**, 5646 (2017).

[21] S. Wang, D. Yin, W. Wang, X. Shen, J.-J. Zhu, H.-Y. Chen, and Z. Liu, Sci. Rep. **6**, 22757 (2016).

[22] A. David, P. Kopecková, J. Kopecek, and A. Rubinstein, Pharm. Res. **19**, 1114 (2002).

[23] N. Sadrieh, J. Brower, L. Yu, W. Doub, A. Straughn, S. Machado, F. Pelsor, E. Saint Martin, T. Moore, J. Reepmeyer, and others, Pharm. Res. **22**, 1747 (2005).

[24] A. I. Baba and C. Câtoi, in *Comparative Oncology* (The Publishing House of the Romanian Academy, 2007).

[25] S. Tiwari, Crit. Rev. Ther. Drug Carr. Syst. **35**, (2018).

[26] S. Deshayes, H. Cabral, T. Ishii, Y. Miura, S. Kobayashi, T. Yamashita, A. Matsumoto, Y. Miyahara, N. Nishiyama, and K. Kataoka, J. Am. Chem. Soc. **135**, 15501 (2013).

[27] J. Wang, W. Wu, Y. Zhang, X. Wang, H. Qian, B. Liu, and X. Jiang, Biomaterials **35**, 866 (2014).

[28] A. Patel, S.Tiwari and P. K. Jha, J. Biomol. Struct. Dyn. **37**, 1545 (2019).

[29] K. Djanashvili, L. Frullano, and J. A. Peters, Chem. - A Eur. J., **11**, 4010 (2005).

[30] A. Matsumoto, N. Sato, H. Cabral, K. Kataoka, and Y. Miyahara, Procedia Eng. **5**, 926 (2010).

[31] J.-Y. Lee, S.-J. Chung, H.-J. Cho, and D.-D. Kim, Adv. Funct. Mater. **25**, 3705 (2015).

[32] J. Xiao, R. L. Melvin, and F. R. Salsbury Jr, J. Biomol. Struct. Dyn. **37**, 982 (2019).

[33] S. Jana and S. K. Singh, J. Biomol. Struct. Dyn. **37**, 944 (2019).

[34] http://www.chemspider.com/Chemical-Structure.60191.html.

[35] M. J. Frisch, G. W.Trucks, H. B. Schlegel, G. E. Scuseria, M. A. Robb, J. R. Cheeseman and X. Li et. al, Gaussian 16, Gaussian. Inc., Wallingford CT, (2016).

[36] C. Lee, W. Yang, and R. G. Parr, Phys. Rev. B **37**, 785 (1988).

[37] S. F. Boys and F. Bernardi, Mol. Phys. **19**, 553 (1970).

[38] C.-G. Zhan, J. A. Nichols, and D. A. Dixon, J. Phys. Chem. A **107**, 4184 (2003).

[39] R. S. Mulliken, J. Chem. Phys. **3**, 573 (1935).

[40] L.-G. Zhuo, W. Liao, and Z.-X. Yu, Asian J. Org. Chem. **1**, 336 (2012).

[41] T. Tsuneda, J. W. Song, S. Suzuki, and K. Hirao, J. Chem. Phys., **133**, 174101 (2010).

[42] J. S. Murray and P. Politzer, Wiley Interdiscip. Rev. Comput. Mol. Sci. **7**, e1326 (2017).

[43] G. Keresztury, J. M. Chalmers, and P. R. Griffith, John Wiey &Sons Ltd (2002).

[44] W. L. Jorgensen, J. Chandrasekhar, J. D. Madura, R. W. Impey, and M. L. Klein, J. Chem. Phys. **79**, 926 (1983).

[45] J. W. Gibbs, *Elementary Principles in Statistical Mechanics Developed with Especial*

Reference to the Rational Foundation of Thermodynamics/by J. Willard Gibbs (New York:: C. Scribner, 1902).

[46] K. Dill and S. Bromberg, *Molecular Driving Forces: Statistical Thermodynamics in Biology, Chemistry, Physics, and Nanoscience* (Garland Science, 2012).

[47] J. L. Banks, H. S. Beard, Y. Cao, A. E. Cho, W. Damm, R. Farid, A. K. Felts, T. A. Halgren, D. T. Mainz, J. R. Maple, and others, Comp. Chem. **26**, 1752 (2005).

[48] F. Leroy, Soft Materials, 11, 231 (2013).

[49] A. Tokatlı, E. Özen, F. Ucun and S. Bahçeli, Spectrochim. Acta A Mol. Biomol. Spectrosc.**78**, 1201 (2011).

[50] E. Scrocco and J. Tomasi, In Advances in quantum chemistry. Academic Press. **11**, 115 (1978).

[51] P. Politzer and J. S. Murray, ChemPhysChem **21**, 579-588 (2020).

[52] N. Okulik and A. H. Jubert, Internet Electron. J. Mol. Des. **4**, 17 (2005).

[53] S. Gunasekaran, S. Kumaresan, R. Arunbalaji, G. Anand, and S. Srinivasan, J. Chem. Sci. **120**, 315 (2008).